Density-functional theory for an electrolyte confined by thin charged walls

Douglas Henderson
Department of Chemistry and Biochemistry, Brigham Young University, Provo, Utah 84602-5700

Paweł Bryk and Stefan Sokołowski
Department for Modelling Physico-Chemical Processes, MCS University, 20031 Lublin, Poland

Darsh T. Wasan
Department of Chemical Engineering, Illinois Institute of Technology, Chicago, Illinois 60616
(Received 15 October 1999)

Results are reported for the primitive model of an electrolyte and for the solvent primitive model of an electrolyte for the case where these fluids are confined by two charged walls. When the walls are thin, the confined electrolyte inside the walls is affected by the charge on both the inside and the outside of the walls. In the case of the primitive model (PM), this system has been studied previously using a singlet integral equation. Our density-functional (DF) study is more general because the fluids inside and outside the walls are constrained to have the same chemical potential and because solvent effects are considered, albeit at a crude level. The singlet integral equation does not consider the chemical potential constraint explicitly. We find that for the low density PM, the DF and integral equation approaches yield, except for a very narrow pore, very similar results. When solvent molecules are considered, the profiles become oscillatory. The co-ion density profiles are particularly interesting because the repulsive electrostatic potential and the effect of the increased pressure in ''pushing'' the co-ions against the wall compete.

PACS number(s): 61.20.−p, 68.10.−m, 68.15.+e, 82.45.+z

I. INTRODUCTION

Lozada-Cassou *et al.* [1–6] have made extensive and important studies of fluids confined by two thin walls. They find that when the walls are thin the fluid inside the walls can be affected significantly by the fluid outside. In particular, it is found that when the fluid is an electrolyte, local charge neutrality between the fluid inside and the inside surface of the wall and between the fluid outside and the outside surface of the wall is not satisfied, except when the two walls have the same electrostatic potential. Of course, overall charge neutrality is always satisfied.

The numerical results of Lozada-Cassou were obtained from the singlet hypernetted chain integral equation for the density profile with the bulk direct correlation function evaluated from the mean spherical approximation (MSA). Lozada-Cassou calls this theory the three-point extension because the coordinates of three particles (two walls and one fluid particle) are employed. We refer to this approach as the singlet theory because the position of only one fluid particle is taken into account. Several studies [7] have shown that for confined (uncharged) fluids density-functional (DF) theory is an attractive alternative. Density-functional theory yields results that are more accurate than those of the singlet theory and are comparable with those of a pair level integral equation approach (a four-point extension in Lozada-Cassou's nomenclature), but is considerably easier to implement.

In our earlier study, we considered only the inside of a slit. This is fine for uncharged systems. However, when Coulomb forces are present, both the inside and outside must be considered. In the present geometry, with a wall with both an inside and an outside, DF theory has the advantage that the fluids inside and outside the pore walls are constrained to have the same chemical potential and this chemical potential is equal to that of the bulk fluid. In the singlet theory, the fluid inside and outside the pore walls are considered to be in equilibrium only through the fact that the same bulk direct correlation function is employed for the integral equations for the fluid inside and outside the pore. Of course, the fluid inside the slit ''knows'' that there is a fluid outside the slit. However, the chemical potential does not enter the formalism explicitly; consequently the fluids inside the pore and outside of it may not, in general, be in chemical equilibrium. This may be only a pedantic problem since in the singlet theory the fluid inside and outside the slit is treated as the same fluid ''wrapped'' around the slit walls. In any case, there is a further problem. The properties of the bulk fluid are defined by the usual Ornstein-Zernike (OZ) equations for the bulk fluid that is the source of the direct correlation function used in the singlet formalism. There is nothing in the formalism to guarantee that the fluid inside or outside the pore has the same chemical potential as the bulk fluid, especially when the bulk OZ equation is solved with a different closure than the singlet equation. In our comparison of DF theory, the results of the singlet theory, and simulations, the singlet theory gives quite good results. It could be argued that this indicates that the singlet theory is satisfying the equality of chemical potentials. However, the singlet results are available only for a low density system where there are no explicit solvent molecules. Our studies of uncharged hard spheres show that the singlet theory is less satisfactory at higher densities, possibly indicative of a problem with the chemical potentials. Of course, in the absence of any approximations the chemical potential would be constant. However, after approximations have been introduced this may not be the case. In contrast, DF theory is formulated in terms of the grand potential and constant chemical potential

is preserved even after approximations are introduced. At the very least, this is a conceptual advantage.

In view of the advantages of DF theory, we feel that it is worthwhile applying this approach to an electrolyte formed by two thin walls. In addition, we consider solvent effects that have not been considered explicitly in Lozada-Cassou's studies. Lozada-Cassou used the *primitive model* (PM) of an electrolyte, where the solvent is modelled as a continuum of dielectric constant ϵ. A sophisticated model of water, i.e., a model of a simple solvent without hydrogen bonding but with a dipole moment, may be also implemented in the framework of a DF approach [8]. However, in this work we consider the most primitive model of a solvent. We use the *solvent primitive model* (SPM), where the ions are charged hard spheres whose Coulomb interactions are attenuated by ϵ and where the molecular nature of the solvent is represented by a fluid of hard spheres.

Although quite crude, this model has been used with success [9,10] in other applications. Admittedly, hard spheres are a poor representation of a solvent but they do recognize the fact that the solvent is composed of molecules that occupy space (they reduce the ''free volume'' to use van der Waals' expression). As a result, the SPM is an advance over the PM of an electrolyte, where the ions are represented by charged hard spheres and the solvent manifests itself only through the presence of ϵ.

Here results are reported for both the primitive and solvent primitive models. For simplicity, we assume that the charged hard spheres (the ions) and the uncharged hard spheres (the solvent molecules) have the same diameter d. This is a purely technical restriction. It can be relaxed and more general studies will be considered in subsequent work.

II. THEORY

We consider a pair of walls of thickness Δ centered at $z=0$ and separated by a distance L. The linear distance perpendicular to the walls is denoted by z. There is symmetry about $z=0$. The inner and outer surfaces of each wall are given the charge densities σ_1 and σ_2, respectively. The corresponding electrostatic potentials are V_1 and V_2. The interaction between the ions is

$$u_{ij}(r)=\begin{cases}\infty, & r<d,\\ \dfrac{q_iq_j}{\epsilon r}, & r>d,\end{cases} \tag{1}$$

where q_i is the charge of an ion of species i and r is the separation of the ions. The interaction between the solvent molecules and between the solvent molecules and the ions is a hard sphere interaction, i.e., Eq. (1) with $q_k=0$. The quantity ϵ is the dielectric constant, which we assume is uniform throughout the entire system and the same for all distances.

The interaction between the ions of species i and the wall is given by

$$u_i(z)=v_i(z)+w_i(z), \tag{2}$$

where $w_i(z)$ and $v_i(z)$ are the electrostatic and the nonelectrostatic van der Waals parts of the external potential, respectively. The van der Waals interaction potential is

$$v_i(z)=\begin{cases}\infty & \dfrac{L-\Delta-d}{2}<|z|<\dfrac{L+\Delta+d}{2},\\ 0 & \text{otherwise.}\end{cases} \tag{3}$$

The electrostatic interaction between an ion and the surface of a wall (or sheet of charge) is given by

$$w_i(z)=\frac{4\pi\sigma q_i}{\epsilon}z', \tag{4}$$

where σ is the uniform charge per unit area, which equals σ_1 or σ_2, as appropriate, and z' is the distance from the surface [i.e., the planes at $|z|=(L\pm\Delta)/2$]. In the SPM, there is no electrostatic interaction between the solvent molecules and the wall. Formally, the solvent molecules are uncharged ions; thus, we can think of the system as a three component system with one species having the charge $q_s=0$.

The electrostatic potential $\Phi(z)$ is determined by Poisson's equation

$$\nabla^2\Phi(z)=-\frac{4\pi}{\epsilon}\sum_i q_i\rho_i g_i(z), \tag{5}$$

where $\rho_i(z)=\rho_i g_i(z)$ is the density profile of an ion of species i and ρ_i is the density of a bulk particle of species i.

Integrating, we obtain for $z>(L+\Delta)/2$,

$$\frac{d\Phi(z)}{dz}=\frac{4\pi}{\epsilon}\sum_j q_j\rho_j\int_z^\infty g_j(t)dt \tag{6}$$

and

$$\Phi(z)=-\frac{4\pi}{\epsilon}\sum_j q_j\rho_j\int_z^\infty (t-z)g_j(t)dt. \tag{7}$$

In obtaining Eqs. (5) and (6), the boundary conditions that $\Phi(z)$ and its derivative vanish at $z=\infty$ has been used.

For $0<z<(L-\Delta)/2$, integrating Poisson's equation yields

$$\frac{d\Phi(z)}{dz}=-\frac{4\pi}{\epsilon}\sum_j q_j\rho_j\int_0^z g_j(t)dt. \tag{8}$$

Because of the symmetry about $z=0$, the boundary condition $d\Phi(z)/dz=0$ at $z=0$ has been used. One further integration yields the electrostatic potential,

$$\Phi(z)=-\frac{4\pi}{\epsilon}\sum_j q_j\rho_j\left[\int_0^z (t-z)g_j(t)dt - \int_0^{(L-\Delta)/2}\left(t-\frac{L-\Delta}{2}\right)g_j(t)dt\right]+V_1, \tag{9}$$

where the boundary condition

$$V_1=\Phi\left(\frac{L-\Delta}{2}\right) \tag{10}$$

has been used. The potential V_2 is given by

$$V_2=\Phi\left(\frac{L+\Delta}{2}\right). \tag{11}$$

Inside the wall, there is no charge. Hence, for $(L-\Delta)/2<z<(L+\Delta)/2$,

$$\Phi(z)=\frac{V_1+V_2}{2}+\frac{V_1-V_2}{2}\left(\frac{L-2z}{\Delta}\right). \tag{12}$$

The charge on each surface of the wall can be obtained from Gauss's law.

Thus,

$$\sigma_1=-\left(\frac{\epsilon}{4\pi}\right)\frac{V_2-V_1}{\Delta}-\sum_j q_j\rho_j\int_0^{(L-\Delta)/2} g_j(t)dt \tag{13}$$

and

$$\sigma_2=\left(\frac{\epsilon}{4\pi}\right)\frac{V_2-V_1}{\Delta}-\sum_j q_j\rho_j\int_{(L+\Delta)/2}^{\infty} g_j(t)dt. \tag{14}$$

Overall charge neutrality

$$\sigma_1+\sigma_2=-\sum_j q_j\rho_j\int_0^{\infty} g_j(t)dt \tag{15}$$

is satisfied. As emphasized by Lozada-Cassou, the charge in the electrolyte in the regions $0<z<(L-\Delta)/2$ and $(L+\Delta)/2<z<\infty$ do not equal σ_1 and σ_2 unless $V_1=V_2$.

For simplicity, we assume that the salt in the electrolyte is symmetric; thus, $q=|q_i|$ and $\rho_1=\rho_2$. The total density of the system is

$$\rho=\rho_s+\rho_1+\rho_2, \tag{16}$$

where ρ_s is the density of the solvent molecules.

Our DF calculations were performed using the theory of Rosenfeld [11] as modified and simplified by Kierlik and Rosinberg [12]. We write only the final density profile equation; the details of this DF theory can be found in their original papers,

$$\begin{aligned}-kT\ln[\rho_i(z)/\rho_{ib}]=v_i(z)&+\left[\frac{\delta F_{\rm HS}^{\rm ex}}{\delta\rho_i(\mathbf{r})}-\mu_{i,\rm HS}^{\rm ex}\right]\\&+q_i[\Phi(z)-\Phi_{\rm bulk}]\\&-kT\sum_j\int\Delta c_{ij}(|\mathbf{r}-\mathbf{r}'|)\Delta\rho_j(z')d\mathbf{r}',\end{aligned} \tag{17}$$

where $F_{\rm HS}$ is the excess free energy functional of a hard sphere system of density ρ, $\mu_i^{\rm ex}$ is the excess (apart from ideal contribution) parts of the chemical potential, $\Delta\rho_i(\mathbf{r})=\rho_i(\mathbf{r})-\rho_i$ and $\Delta c_{ij}(r)$ are the short-ranged parts of the direct correlation functions resulting from Coulombic interactions. The most widely used expression to evaluate these functions is the MSA result, which is of reasonable accuracy and yields the following analytical expressions [13]:

$$kTc_{ij}(r)=\begin{cases}-\dfrac{q_iq_j}{\epsilon}\left[\dfrac{2A}{d}-\left(\dfrac{A}{d}\right)^2r-\dfrac{1}{r}\right] & r<d\\ 0 & r>d.\end{cases} \tag{18}$$

In the above $A=x^{-2}[x^2+x-x(1+2x)^{1/2}]$, and $x=(4\pi\beta d^2/\epsilon)\Sigma_i\rho_{ib}q_i$.

The main deficiencies of the MSA theory are well known [14]. In order to improve the theory, one should use a more elaborate theory, for example, the generalized MSA or GMSA theory [15], or the hypernetted chain (HNC) theory [16]. However, similarly to other authors, here we shall use only the MSA theory as a first approximation.

For the hard sphere part, i.e., for $F_{\rm HS}^{\rm ex}$, we adopt one of the most accurate nonlocal functionals, i.e., the Kierlik-Rosinberg version of the DF theory [12]. Because this theory is quite standard, we refer the reader to their papers.

Our numerical procedure involves the numerical solution of Eq. (17), together with the equations defining $\Phi(r)$, using a standard Picard iteration method. The grid size that we employed was $0.025d$. When the norm of the difference vector between the kth and $(k+1)$th iterates of the $g_i(r)$ was less than 10^{-7}, the iteration was deemed to have converged.

It is convenient to introduce reduced or dimensionless units in our calculations. The reduced temperature is

$$T^*=\frac{k\epsilon d}{q^2}T, \tag{19}$$

where k is the Boltzmann constant. The reduced charge densities on the surfaces of the wall are

$$\sigma_i^*=\frac{\sigma_i d}{q}, \tag{20}$$

and the reduced potential is

$$\Phi^*(z)=\beta q\Phi(z), \tag{21}$$

where $\beta=1/kT$. The value for T^* that we use is the value chosen by Torrie and Valleau [17],

$$1/T^*=1.6808, \tag{22}$$

or, equivalently, a reduced charge of

$$q^*=\frac{1}{\sqrt{T^*}}=\left(\frac{\beta q^2}{\epsilon d}\right)^{1/2}=1.296. \tag{23}$$

This corresponds to an aqueous solution at room temperature with a core diameter $d=4.25$ Å.

III. RESULTS AND DISCUSSION

In Fig. 1 we show the results for an 1:1 PM electrolyte that has been studied by Lozada-Cassou, cf. Fig. 6 of Ref. [5]. The reduced charge density of each plate is $\sigma^*=0.013\,529\,11$, the reduced plate width is $\Delta/d=1$. The reduced concentration of anions and cations is $\rho_i d^3=0.000\,462\,4$ (0.01 M) and $1/T^*=1.6808$. Figure 1(a) corresponds to Fig. 5(a) from Ref. [5]. The solid and dashed lines give the results for the counterions and co-ions, respectively, obtained from DF theory. For Fig. 1, the HNC/MSA

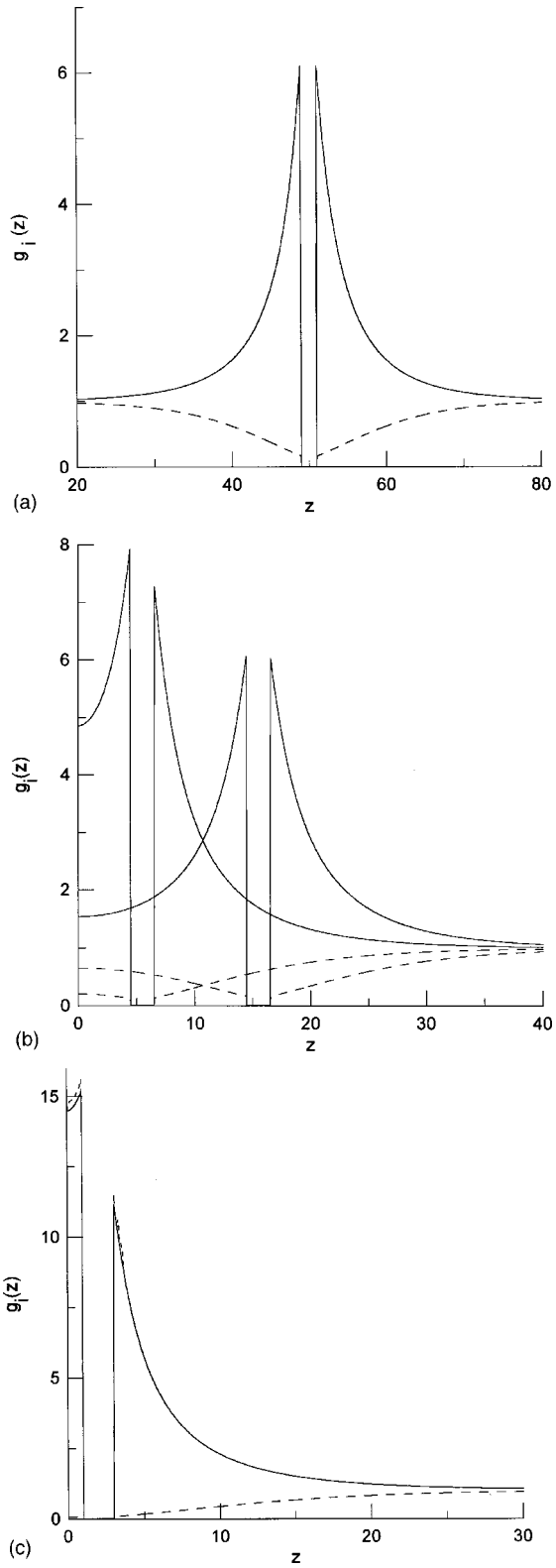

FIG. 1. Density profiles for ions in a 1:1 PM at a concentration of 0.1 M. The charge density on the wall is $\sigma_1^*=\sigma_1^*=0.013\,529\,11$. (a) and (b) The solid and dashed lines give the counterion and co-ion profiles, respectively. (a) $L=50.5d$; (b) we have two sets of results for $L=5.5d$ and for $L=15.5d$. (c) $L=2d$ and only the counterion profiles are plotted. (c) The solid and dashed curves give the DF and HNC/MSA results, respectively. The wall width Δ equals d.

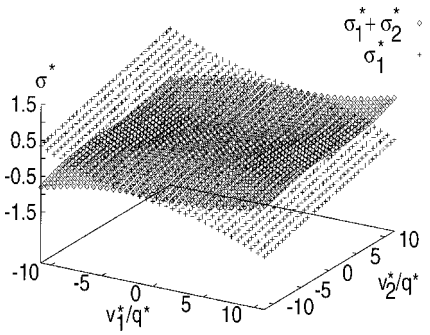

FIG. 2. A plot of the total charge $\sigma_1^*+\sigma_2^*$ on the plates and the charge on the inner plate σ_1^* vs the potentials of the inner and the outer plates for the PM. The quantities V' are V^*/q^*. The reduced density of the anions and cations is 0.000 462 4 (0.01 M), $L=2d$, and $\Delta=d$.

profiles, obtained by Lozada-Cassou, are indistinguishable from those resulting from DF theory; therefore, the HNC/MSA results are not plotted here. The situation in Fig. 1(b) is similar. Lozada-Cassou has plotted the curve only for $L=5.5$; we have added the results for a wider pore. Note that Lozada-Cassou's definition of τ (the pore width) is shifted by $\Delta/2$ with respect to L; $L=\tau+\Delta/2$. Thus, there are almost no differences between the HNC/MSA and DF approaches for the case of Figs. 1(a) and 1(b). However, for a narrower pore, shown in Fig. 1(c) we see some differences. Here, only the profiles of the counterions are shown. The solid lines and dashed lines give the DF and HNC/MSA results, respectively. The differences are more pronounced inside the pore; however, they are still small. However, the fact that the concentration is quite low is to be kept in mind. From our calculations for hard spheres in a pore, we know that DF theory is more accurate than the HNC/MSA approach.

To summarize the results in Fig. 1, when L is sufficiently large, the profiles inside and outside are almost symmetric [Fig. 1(a)] and the ''local electoneutrality condition'' is ''almost'' satisfied. The profile inside the pore of width $L=15.5$ [Fig. 1(b)] is still ''almost'' the same as the profile outside; indeed, the profiles for this pore are almost identical as those for $L=50.5$ [Fig. 1(a)]. Decreasing L results in increasing values of the contact values of the counterions profiles with the profile of counterions inside the pore being higher than the counterion profile outside the pore. Only for a very narrow pore do we observe more pronounced differences between the HNC/MSA and DF profiles [Fig. 1(c)].

In Fig. 2, we show plots for the total charge $\sigma_1^*+\sigma_2^*$ of the plates and the charge on the inner plate and σ_1 as functions of the potentials of the inner and the outer plates for the 0.01 M PM for the geometry of Fig. 1(c). The local electroneutrality condition is satisfied along the diagonal $V_1=V_2$.

The interaction force between two pore walls, as defined by Lozada-Cassou, is

$$f(L)/kT=\sum_i \left\{ \rho_i(z=L-\Delta-d/2)-\frac{2\pi}{\epsilon}\left[\int_{d/2}^{L} dz \sum \rho_i(z)\right]^2 - \sum \rho_i(z=L+\Delta+d/2) + \frac{2\pi}{\epsilon}\left[\int_{L+d/2}^{\infty} dz \sum \rho_i(z)\right]^2 \right\} \tag{24}$$

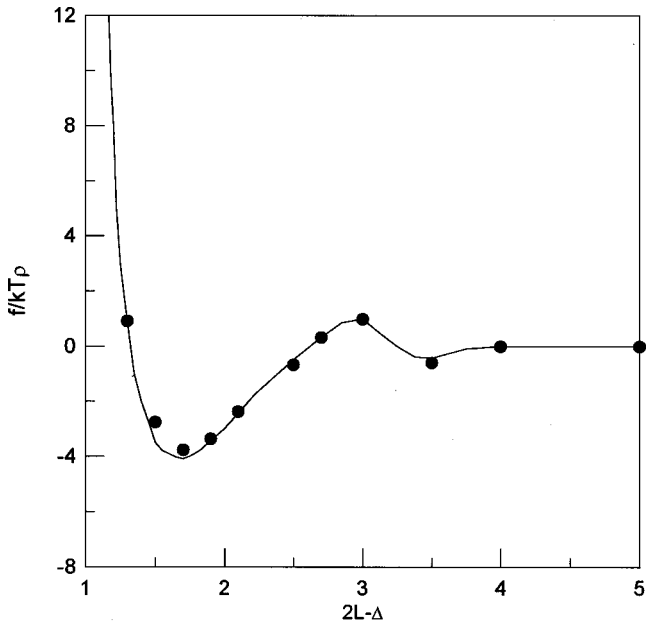

FIG. 3. The force between two walls of a slitlike pore vs the pore width. The points give the MC results and the curve gives the DF results. In this calculation $\Delta = 20d$, the charge density is $\sigma_1^* = \sigma_2^* = 0.306\,666$, and the ionic densities are $\rho_i d^3 = 0.044\,894\,9$ (a concentration of 0.971 M).

for a 2:2 electrolyte (PM). The simulations of Valleau *et al.* [18] were performed for ions in a slit with a very wide wall, i.e., there is no ''outer world,'' and no outer solvent. Thus, in our calculations, we used a rather wide wall, $\Delta = 20d$; the charges were $\sigma_1^* = \sigma_2^* = 0.306\,666$ and the concentration was 0.971 M (the reduced densities of the anions and cations were $\rho_i d^3 = 0.044\,8949$, cf. Fig. 8(a)) of Ref. [5]. The points are the Monte Carlo (MC) simulation and the solid line give the DF results; DF theory gives very satisfactory results. We have also made calculations for a width of $\Delta = 10d$ and found that the $10d$ and $20d$ DF results are virtually identical. Both thicknesses correspond to an infinitely thick wall. Obviously, if Δ is large enough (infinite), the local electoneutrality condition is always satisfied, independently of the values of the charges (or potentials) on both plates forming the wall. In such a case, the third and fourth terms in the last equation are just those for an infinitely wide pore, or for a single wall. For the states considered, $10d$ and $20d$ are infinite. Note that Lozada-Cassou's discussion [5] about the ''artificial imposition of the local electroneutrality condition'' in the simulations by Valleau *et al.* and also in some earlier DF calculations does not apply to those studies because only a single slit, without an outer solution was used. Their model corresponds to the model of Lozada-Cassou, the model used here, with an infinitely thick wall and local neutrality always applies. Returning to Fig. 3, we stress the good agreement with the simulation studies.

We present some results for a system for which $V_1 = V_2$ (where local electroneutrality applies) in Fig. 4. Three values of the potential $V^* = q^*$ (curves labeled 1) $V^* = 3q^*$ (curves labeled 2) and $V^* = 5q^*$ (curves labeled 3). Figures 4(a) and 4(b) give the co-ion and counterion profiles, respectively. The geometry is the same as that for Fig. 1(c). The reduced densities for the co- and counterions are equal to 0.052 (i.e.,

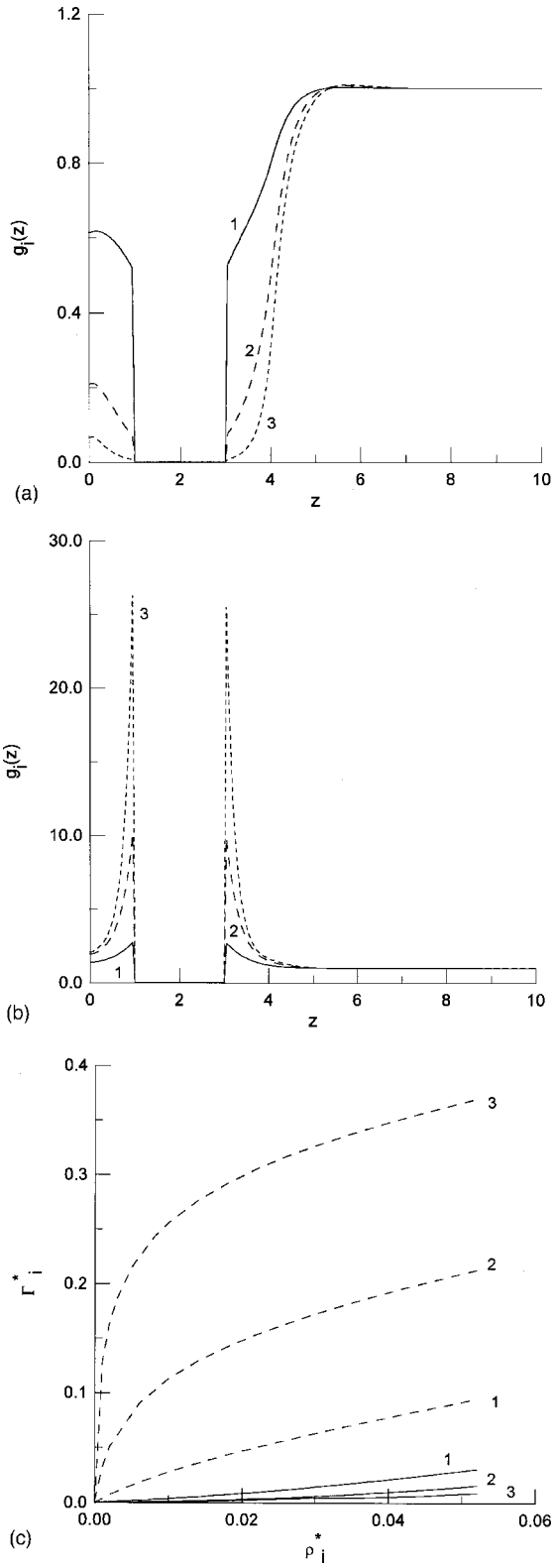

FIG. 4. DF calculations for the PM of the coion (a) and counterion profiles (b) and the adsorption isotherms (c). The geometry is $L = 2$ and $\Delta = d$. (a) and (b) The ionic reduced densities are 0.052 for each species. Local electoneutrality conditions $V_1 = V_2$ have been used. For curves 1,2,3, respectively, the values of the potential are $V^* = q^*$, $3q^*$, and $5q^*$. The geometry is the same as in Fig. 1(c). For easier viewing (c) the co-ion adsorption isotherm 2 has been multiplied by 2 and the co-ion adsorption isotherm 3 has been multiplied by 5.

the concentration is slightly higher than 1 M). Figure 4(c) shows the adsorption isotherms $\Gamma_i^* = \Gamma_i d^2$, $\Gamma_i = \int dz \rho_i(z)$. In Fig. 4(c) the solid and dashed lines, respectively, give the coion and counterion isotherms. The numbers 1, 2, and 3, refer to $V^*/q^* = 1$, 3, and 5. Note that the isotherms 2 and 3 for the co-ion (solid lines) have been multiplied by 2 and 5, respectively, for easier viewing. An increase of the potential leads to an increase of the adsorption of the counterions. In contrast, the adsorption of co-ions decreases with increasing potential. The structure of profiles of the co-ions and counterions is rather featureless and is not shown; only one peak is seen at the two walls. Here the ion concentration is much higher than that for Fig. 1(c); however, the differences between the distribution functions of the counterions inside and outside are smaller than at low concentrations. This, presumably, is due to the fact that the screening length for the electrostatic interactions decreases as the concentration increases. As a result, the ''effective'' thickness of the wall increases with increasing concentration and, for a fixed thickness, the electrolytes inside and outside the pore tend to become independent of each other.

We now proceed to the results for ions plus the primitive solvent. In Fig. 5 we show the counterion, Fig. 5(a), and solvent, Fig. 5(b), profiles for the constant charge condition. The geometry, charges, and ionic densities are the same as in Fig. 1(c) i.e., the reduced charge density of each plate is $\sigma^* = 0.013\,529\,11$, the reduced plate separation is $\Delta/d = 1$ and $L = 2d$. The reduced concentration of the anions and cations is $\rho_i d^3 = 0.000\,462\,4$ (0.01 M) and $1/T^* = 1.6808$, $L = 2d$. The calculations have been carried out at three reduced solvent densities 0.1, 0.5, and 0.7. In addition, we have also displayed here the curve for zero solvent concentration [taken from Fig. 1(c)]. With an increase of the solvent density we observe the development of a layered structure in the ionic density profiles. At zero and at low solvent densities, the density profiles exhibit a long-ranged decay, due to the long inverse Debye parameter at low concentrations; the presence of the solvent ''decorates'' this decay. At high solvent densities, the layered structure inside the pore develops with a second local density peak at the pore center. At the highest solvent density, there are several layers outside the pore. This increase in the layered structure is quite usual in liquid-state theory.

Figures 6 and 7 show further SPM results. In Figs. 6 and 7, respectively, density profiles and adsorption isotherms are plotted. The geometry of the system is the same as in Figs. 1(c) and 5; however, in Fig. 7 the ionic densities are much higher, $\rho_i d^3 = 0.052$ (a concentration of the order of 1 M). The calculations were performed under constant potential conditions (i.e., the local electroneutrality condition is satisfied). We have set the potentials V_1 and V_2 to be $V_1^* = V_2^* = 3q^*$. Four solvent densities have been considered; the labels 1, 2, 3, and 4 refer to different solvent densities, see the caption. Figures 6(a)–6(c) show the counterion, co-ion, and solvent profiles, respectively. At low solvent densities, the co-ion profiles show a depletion at the walls, whereas at higher solvent densities, this depletion converts into a maximum. Increasing the solvent density ''pushes'' the ions and solvent molecules against the wall. This is most obvious in the co-ion profiles because the potential on the wall is acting in the opposite direction, pushing the co-ions away from the wall. At low densities, the electrostatic effect dominates whereas at higher densities, the pressure effect becomes significant.

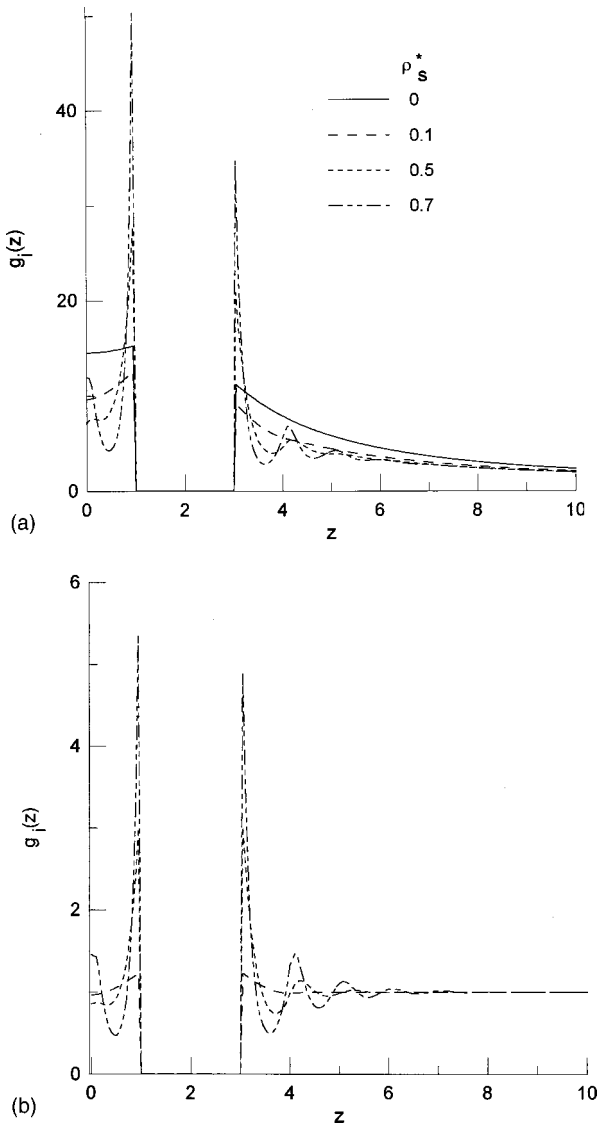

FIG. 5. Counterion (a) and solvent (b) density profiles obtained using the SPM. The calculations are for a reduced charge density on each plate of $\sigma^* = 0.013\,529\,11$, the reduced plate separation is $\Delta = d$; $L = 2d$. The reduced concentration of anions and cations is $\rho_i d^3 = 0.000\,462\,4$ (0.01 M) and $1/T^* = 1.6808$. The solvent reduced densities are 0, 0.1, 0.5, and 0.7; (a) this code is displayed.

Figure 7 shows some adsorption isotherms plotted as functions of the ionic densities. The adsorption isotherms of solvent, Fig. 7(c), are plotted vs ionic densities. Increasing the ionic densities increases the adsorption of the ions. This is to be expected; if there are more ions, more will be adsorbed. Increasing the ionic densities has little effect on the solvent adsorptions because the ionic density is small compared to the solvent density. The adsorption of the solvent molecules and of both the counterions and co-ions increases with increases with increasing solvent density because of the increased ''pushing'' with increased density.

IV. SUMMARY

We have applied DFT to investigate an electrolyte in a pore formed by charged walls of varying thickness with the

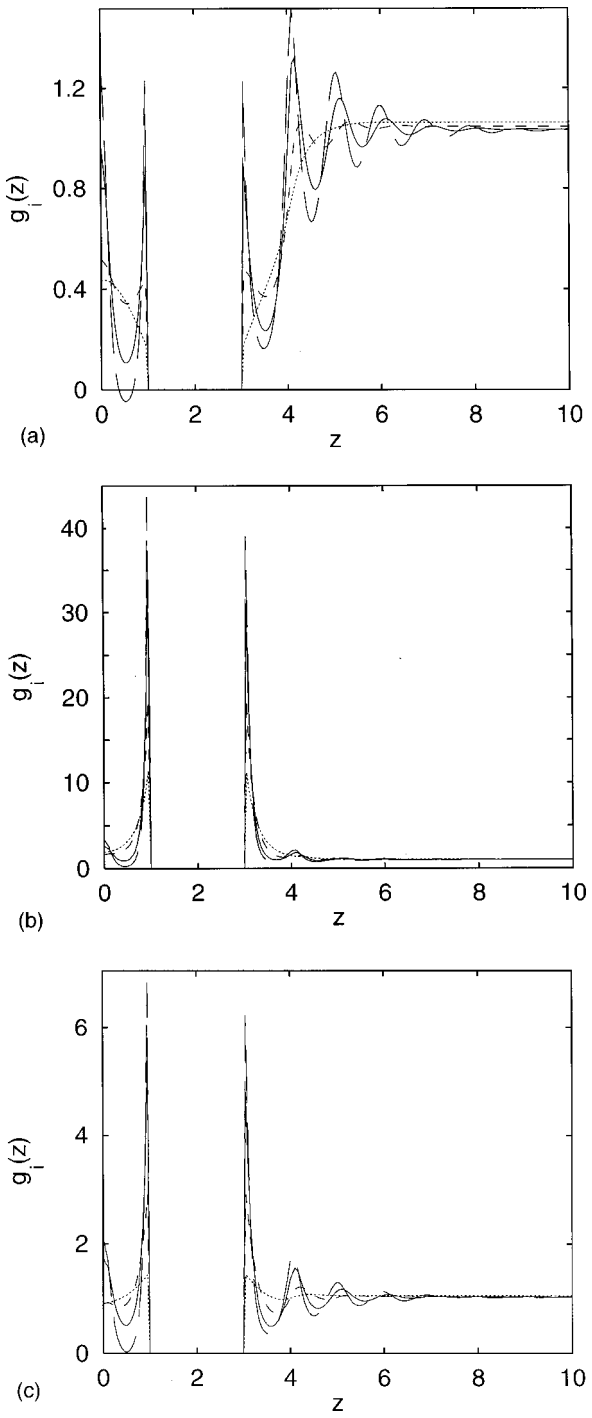

FIG. 6. SPM density profiles of the co-ions (a), counterions (b), and the solvent molecules (c). The geometry of the system is the same as in Figs. 1(c) and 5. The calculations performed with constant potential boundary conditions $V^*=3q^*$. The ionic densities are $\rho_i d^3=0.052$. The lines labeled 1, 2, 3, and 4 correspond to bulk reduced solvent densities equal to 0.7, 0.6, 0.4, and 0.1, respectively.

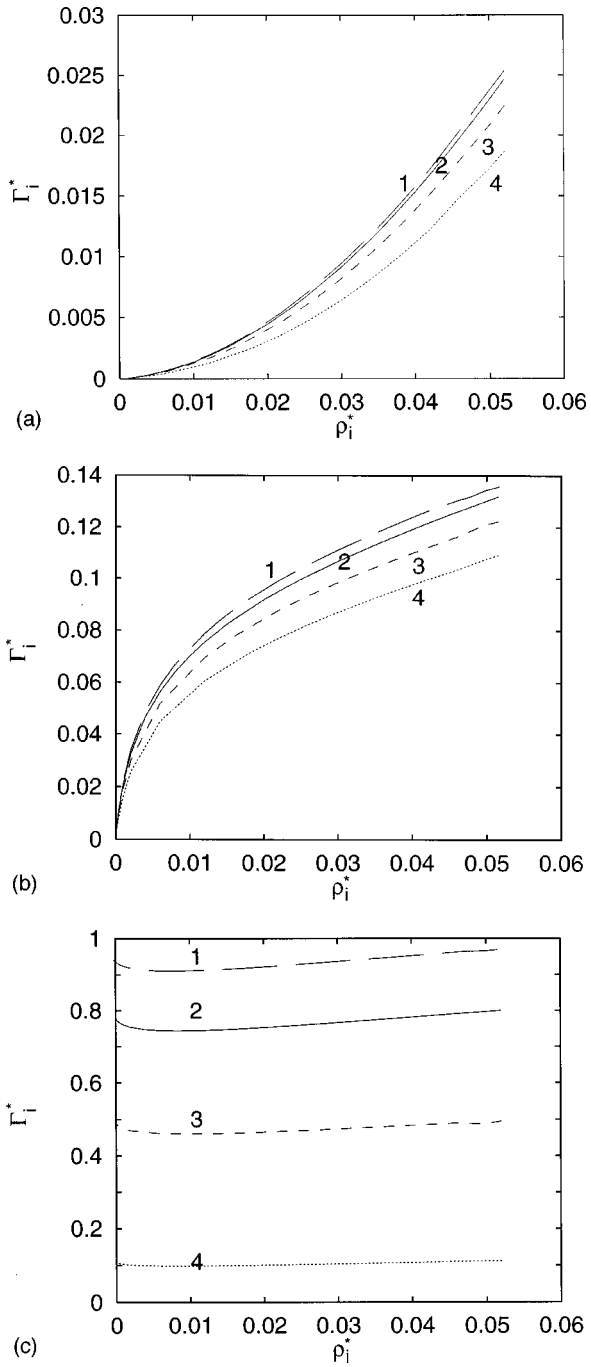

FIG. 7. Adsorption isotherms of co-ions (a), counterions (b), and solvent molecules (c) for the system with the same geometry and electrostatic potential as in Fig. 6. The isotherms are plotted vs ionic density $\rho_i d^3$, $i=1$ or 2. The different lines refer to different bulk solvent densities; the numbers 1, 2, 3, and 4 have the same meaning as in Fig. 6.

fluid inside and outside the wall being in equilibrium. We have studied the profiles and adsorption isotherms both for a continuum solvent and a molecular solvent. For the case of the continuum solvent, the electrolyte is a low density system and the DFT results are very similar to those of the integral theory of Lozada-Cassou. Both the integral equation and DFT results are in gratifyingly good agreement with the simulation results.

When a molecular model of the solvent is introduced, the density of the electrolyte can be large. Under such conditions, we expect that DFT will be much more accurate than the singlet level integral equations. We have already seen this for uncharged hard spheres in a pore [19]. Of course, as was done in Ref. [19], good results can be obtained by using a pair level integral equation but at a considerable cost in computational complexity. Previous comparison of DFT with simulations for the case of an infinitely thick charged

wall have shown DFT to be reliable. We have every reason to expect this to be the case for thinner walls.

ACKNOWLEDGMENTS

The work of D.H. was supported in part by the National Science Foundation (Grant Nos. CHE96-01971 and CHE98-13729), by the donors of the Petroleum Research Fund, administered by the American Chemical Society (Grant No. ACS-PRF 31573-AC9), and by a NATO High Technology Collaborative Research Grant (Grant No. HTECH, CRG 972915). S.S. acknowledges support from KBN under Research Grant No. 3T09A 082 16.

[1] M. Lozada-Cassou, J. Chem. Phys. **80**, 3344 (1980).
[2] M. Lozada-Cassou and E. Diaz-Herrera, J. Chem. Phys. **92**, 1194 (1990).
[3] M. Lozada-Cassou and J. Yu, Phys. Rev. Lett. **77**, 4019 (1996).
[4] M. Lozada-Cassou, W. Olivares, B. Sulbarán, and Y. Jiang, Physica A **231**, 197 (1996).
[5] M. Lozada-Cassou, W. Olivares, and B. Sulbarán, Phys. Rev. E **53**, 522 (1996).
[6] M. Lozada-Cassou, in *Fundamentals of Inhomogeneous Fluids*, edited by D. Henderson (Dekker, New York, 1992), Chap. 8.
[7] R. Evans, in *Fundamentals of Inhomogeneous Fluids* (Ref. [6]), Chap. 4.
[8] T. Biben, J. P. Hansen, and Y. Rosenfeld, Phys. Rev. E **57**, R3727 (1994).
[9] D. Henderson and M. Lozada-Cassou, J. Colloid Interface Sci. **114**, 180 (1986).
[10] Z. Tang, L. E. Scriven, and H. T. Davis, J. Chem. Phys. **97**, 494 (1992); **100**, 4527 (1994).
[11] Y. Rosenfeld, Phys. Rev. Lett. **63**, 980 (1989).
[12] E. Kierlik and M. L. Rosinberg, Phys. Rev. A **42**, 3382 (1990); **44**, 5025 (1991).
[13] E. Waisman and J. L. Lebowitz, J. Chem. Phys. **52**, 430 (1970); **56**, 3093 (1972).
[14] L. Blum, in *Theoretical Chemistry: Advances and Perspectives*, edited by D. Henderson (Academic Press, New York, 1980), Vol. 6, p. 1.
[15] J. S. Høye, J. L. Lebowitz, and G. Stell, J. Chem. Phys. **61**, 3252 (1974).
[16] J. C. Rasaiah and H. L. Friedman, J. Chem. Phys. **48**, 2742 (1968); **50**, 3965 (1969); J. C. Rasaiah, Chem. Phys. Lett. **7**, 260 (1970); J. Chem. Phys. **52**, 704 (1970).
[17] G. Torrie and J. P. Valleau, J. Chem. Phys. **73**, 5807 (1980).
[18] J. P. Valleau, R. Ivkov, and G. M. Torrie, J. Chem. Phys. **95**, 520 (1991).
[19] D. Henderson, S. Sokolowski, and D. T. Wasan, J. Stat. Phys. **89**, 233 (1997); J. Phys. Chem. B **102**, 16 (1998).